Steam-Powered Sensing: Extended Design and Evaluation *

ISI Technical Report ISI-TR-2011-670

Chengjie Zhang Affan Syed Young H. Cho John Heidemann
USC/Information Sciences Institute

Feb. 2011

Abstract

Sensornets promise to extend automated monitoring and control into industrial processes. In spite of great progress made in sensornet design, *deployment and operational cost* impedes use of sensornet in many real-word scenarios—these challenges are so great that industries often continue with infrequent, manual observations over automation, even for key business processes. In this paper we propose two novel approaches to reduce system deployment cost, and test those approaches in a real-world monitoring of steam pipelines in oil industry. First, we make use *temperature differences* between the pipeline's surface and the atmosphere *reliable source of harvestable energy* for sensornet operation. We demonstrate that for temperature differences of 80 ℃ or more, batteryless operation is possible using only a low-cost 40x40mm thermoelectric generation module; thereby significantly reduce costs of deployment and operation. Second, we show that *non-invasive sensing* can infer blockages in water and steam pipelines, and partial blockages in steam pipelines. Non-invasive sensing eliminates the need to pierce the pipeline, greatly reducing deployment cost. Finally, we evaluate our "steam-powered sensing" system in *an application monitoring blockage in steam pipeline chokes in a production oilfield*. To our knowledge, this is the first industrial field sensornet deployment that employ non-solar energy harvesting. To broaden our results, we also show our approaches also apply to blockage detection in lower temperature water pipelines through laboratory experiments.

*This research is partially supported by CiSoft (Center for Interactive Smart Oilfield Technologies), a Center of Research Excellence and Academic Training and a joint venture between the University of Southern California and Chevron Corporation.

1 Introduction

Automated monitoring and control of industrial processes are becoming increasingly important as industrial operations grow in complexity and size. Since 1960s, supervisory control and data acquisition (SCADA) systems have been used to automate monitoring and control of industrial processes in applications ranging from water management, power grids, chemical refining and processing, to oil production [14]. Today, SCADA systems are a multi-billion-dollar-per-year industry, and the need for wireless and distributed sensornet techniques is growing.

One effective use of SCADA systems can be seen in oil industry. While the fabled "gusher" produces oil from internal pressure, in most cases this kind of primary production can only extract a fraction (5–10%) of oil in the ground. Today many older fields depend on *secondary* production techniques, where water, steam, or CO_2 is injected to force out oil, allowing extraction to approach 30–60% of reserves. While such techniques are essential to meet energy demands, the key limiting factor is *cost*, not technology. The cost of automation needed for effective secondary production guide SCADA and sensornet deployments. Although oil companies have great technical sophistication, so-

lutions as simple as monthly human monitoring of a service are often seen as sufficient and more cost effective than expensive automation. Even with relatively inexpensive hardware, the cost to install the sensor to monitor a pipe can easily top US$10k to power it and tap the pipe.

In this paper we propose an *inexpensive* sensornet system to monitor steam injection in oilfields. We directly address the cost of current approaches through two contributions. First, we demonstrate a new approach to *harvest energy from temperature differential* inherent in the phenomena we are studying. We exploit the Seebeck effect induced by heat that is naturally present in the steam injection system to generate enough power for sensor nodes, eliminating any need for external power or batteries. Although many prior systems have demonstrated energy harvesting, they have typically been from solar power or vibration. We are the first to exploit heat for large-scale industrial sensing and to show operation solely on harvested power without batteries operating as buffer. Our approach is important for extended operation where solar is ineffective (for example, the north shore of Alaska) vibration is insufficient, and batteries are not easily replaceable.

Second, we employ *non-invasive sensing techniques* to detect problems in steam distribution. Current approach to determine steam flow rate typically requires direct measurement of differential pressure within the pipeline. Installation of pressure sensing devices require production halt and piercing of the pipelines; costing thousands of dollars. We, instead, observe that external temperature observation is sufficient to detect problems such as blockage or flow constriction, and with care, even to infer flow rates, *provided* we can observe at multiple locations. We argue that pervasive industrial sensing requires this sort of non-invasive sensing to reduce deployment cost.

Our final contribution is to demonstrate that our approach to non-invasive, steam-powered sensing works as a complete system, through both laboratory experiments and field tests. Although low-power sensing and energy harvesting have been demonstrated before, we are the first to demonstrate an integrated targeted at a new application. To provide this system, we added a custom thermoelectric energy harvesting/conditioning unit and a custom amplification board with calibrated thermocouples to sense temperature using a standard Mica-2 motes, and developed new detection algorithms that run on this platform.

Although we validate our approach with a very specific oilfield deployment, the approaches are applicable to a wide range of industrial sensing. Many industrial processes have moderate or large temperature differentials that could support energy harvesting, and non-invasive sensing is important to bring the cost of sensing in line with inexpensive communications and computation.

2 Problem Statement and System Overview

In this section we describe the sensing needs in modern oilfields followed by an overview of our prototype sensor node. In later sections we cover the details of our energy harvesting (Section 3) and sensing algorithms (Section 4).

2.1 Sensing needs in an Oilfield with Secondary Production

Most modern oilfields employ *secondary production*, where water, steam, or CO_2 is injected into the ground to release otherwise difficult to extract oil. In addition to helping release trapped oil, injection helps maintain underground pressure to avoid ground subsidence, a potential environmental problem and a source of damage to wells. While secondary production is essential to extracting oil in older fields where the natural pressure is insufficient for primary (unaided) production, it greatly adds to the complexity of the field.

Figure 1 depicts a simplified oil production scenario with steamflood-based secondary production. Steam is produced at a central site, (often a co-generation facility that also provides electrical power) and is distributed throughput the field at high temperature and pressure (250 ℃ and 5000k Pa or more) [5]. Steam in the distribution network is actually an ap-

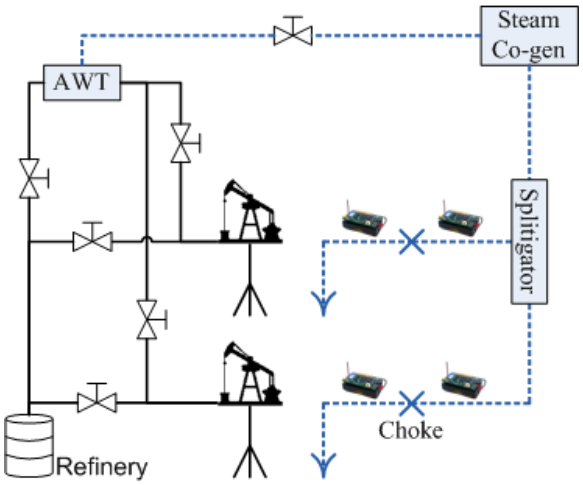

Figure 1: Steam injection (right) and oil production (left) in oilfield.

proximate mix of 70% steam and 30% water. Maintaining this ratio (called *steam quality*) is important to control injection characteristics. Special devices called *splitigator* are necessary to maintain steam quality at any pipeline branch. In addition, steam pressure is regulated by a *choke*, a small, controlled-size hole (about 1 cm or more in diameter) just before an injection well. In the ground, steam helps heat oil and bitumen, and provides fluid pressure to release and drive oil to a nearby production well.

On the production side, an oil well extracts oil from underground and sends it downstream towards the refinery. It is important to monitor each well's production, both to understand the field's behavior, and because individual wells are often leased from different owners, each of whom must be paid. In some fields, each well's production is individually instrumented. However, in most production fields, each production line is directed to an *automatic well testing* (AWT) facility before being merged in order to reduce cost. The AWT allows multiple wells to share common monitoring hardware for periodic production audits. Wells also occasionally need to be flushed with steam to remove blockages, so the steam distribution system connects to the AWT, and a production well can be isolated and its flow reversed to inject steam when needed.

This brief description highlights the essential role instrumentation plays in an oilfield. Steam quality must be monitored in the steam distribution network; flow rates at injection wells and chokes must be observed; well monitoring is essential at the production side; the ability to inject steam in production systems means the injection and production sides are cross-linked and must be monitored for leaks. Yet all this work must be accomplished cost-effectively, even for wells that produce only a few barrels of oil per day, and in fields that have hundreds or thousands of production and injection wells!

2.2 Target Problem: Blockage at the Steam Injection Choke

In this paper we focus specifically on the problem of *blockage at the injection-well choke in a steamflood field*. We define *blockage* as the decreasing of the choke's cross section due to obstructions. Field engineers report that choke blockage is a serious problem in field operation. Chokes are easily clogged by small objects because their small bore is a natural point of blockage. Sources of blockage occur naturally in a steam distribution system due to scaling and corrosion in the pipe, buildup of any impurities or mineral content in the water, and aging of the network and choke. Partial or total blockage at a choke is a serious problem because it alters the steam injection rate, throwing off field management, reducing production, and potentially eventually causing ground subsidence.

Although our current work focuses of blockage at the choke for steamflood fields, we expect that the work also applies to several related problems as well. Other points of operational concern include splitigator operation and AWT monitoring; both could use systems similar to ours. We focus on steamflood systems, but we also show that our sensing algorithm applies to waterflood networks (Section 5.6), and we believe that our energy harvesting system could be adapted for different thermal conditions.

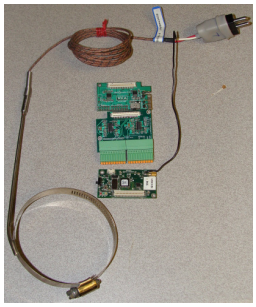

(a) A mica2, a custom amplifier board, a helio-mote and a hose-clamp thermocouple.

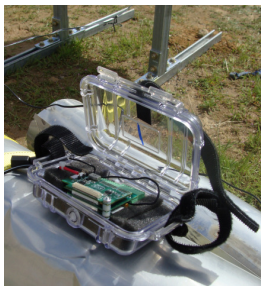

(b) Deployed mount, in a pelican box with lid open.

Figure 3: Mote system hardware.

2.3 System Overview

The goal of our sensing system is to detect blockages at the choke of steam injection wells, and to do so at a cost much lower than current invasive sensing. We next briefly review the hardware and software we have taken into the field to evaluation solutions to this problem.

Figure 2 shows our system in the field deployed in March 2010, with a logical diagram on the left and a photograph of the deployment on the right. Each sensor node in our system includes a mote with two temperature sensors, a thermal energy harvester, and a wireless network connection. Figure 3 shows a deployment with two such sensor nodes and a base station that is connected to the field SCADA system. We review the hardware and software below, and discuss details of this field experiment in Section 5.7. By comparison, Figure 16 shows as a current invasive pressure sensor; we compare deployment costs of our approach to current approaches in Section 5.8.

Each sensor node consists of a compute platform based on a Mica-2 running TinyOS-1. Figure 3(b) shows a mote packaged for field deployment, and 3(a) individual system components and sensors. The sensors themselves are NANMAC J-type thermocouples with hose clamps to attach to the pipeline; Section 5.3 discusses the care that must be taken to get accurate, calibrated temperature readings. Because the voltage output by thermocouples is quite small (less than 15 mV), we add a custom amplification board to boost this signal 100-fold. The whole package is powered by a custom-built thermo-electric generator described in Section 3.

Software on our sensor node includes our new problem detection algorithm (described in Section 4), We run the sensing algorithm locally on the mote and report alerts as they occur to the field SCADA system via the base station. In addition, we log temperature over the radio to the base station, and locally to flash memory for debugging and long-term analysis. In our field experiments we disable logging to flash as described in Section 5.2, but in operation, we would expect local logging to serve as backup in case of temporary network outages.

The base station should be a devices with wireless communication with the sensor nodes that bridges data into the field network and SCADA system. In principle, a mote with a wired network connection, or a multi-hop mote network could service this purpose. We do not currently have permission to integrate with the field SCADA system, so for our experiments our base station is a mote that connects directly to a laptop that logs data to disk.

2.4 Future System Design

Although we have built and tested our prototype system, work remains before the system can be fielded for long term operation. Open issues include fully weatherizing the packaging and fully integrating it with field-wide SCADA systems. In addition, additional packaging work would be required to insure the system is explosion proof (Class I, Division 1) to be safe for use near production wells.

3 Steam-Power: Harvesting Thermal Energy

We now describe our motivation and design choices to build a energy harvesting system exploiting the thermal energy present in the oilfield's steam distribution network. This "steam-powered" system will then

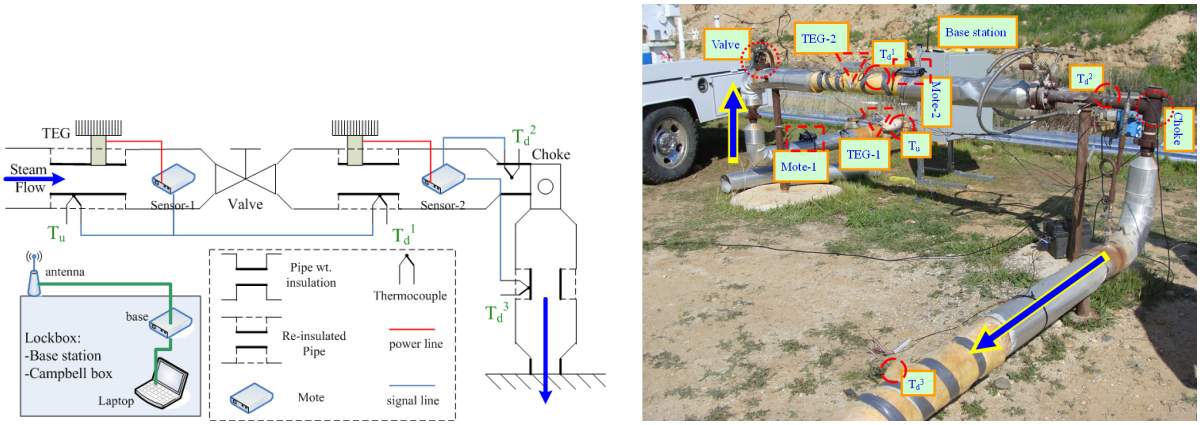

(a) Logical view of deployment.

(b) Physical view of deployment.

Figure 2: March 2010 field deployment of our sensing system.

provide the energy to power the blockage-sensing system we describe in Section 2.3.

3.1 The Opportunity

The main reason for injecting steam into certain secondary production oil field is so that heat from steam can cause the crude oil to drain into the underground reservoir. The collected oil in the reservoir is then pumped out from the well. The goal of our project is to persistently monitor the flow of steam into the injection sites and report any problems when they occur. While framing our research problem, we observed that heat from steam can be harvested to sufficiently operate our sensors without any external power source. In our system *steam-power* is obtained by exploiting the *Seebeck effect* to generate electricity from a temperature differential. Steamflood pipes operate at around 260 ℃, while the ambient temperature averages from 0–38 ℃ over the course of the year at our location, providing a significant temperature differential. An electric circuit converts this temperature differential into a flow of charge with a small voltage differential; many such circuits in parallel form a thermoelectric generator (TEG) to provide usable voltage and current [15, 21]. While prior work has looked at TEG for automotive applications or to augment other power sources, we are one of the first to look at powering sensors in production oil field application. Also, due to efficient TEG, high temperature of the steam, and a large thermal mass of the pipelines, our prototype sensor node is the first of its kind operated directly off the energy harvester without a use of energy buffers such as batteries. We will discuss other TEG related work in more detail on Section 6.1.

Although we explore TEGs to monitor a steam distribution network, many industrial applications have temperature differentials that can be tapped, including many pipeline systems, many systems with engines or motors (even the ones that do not directly produce electricity) and exothermic chemical processes. Although the high temperature differential in our scenario provides significant energy with a relatively small TEG, other scenarios can use larger surface areas coupled with energy buffers.

Our system demonstrates the concept of *energy sufficiency*, beyond energy-efficiency, for ambient-powered sensor networks. Energy-sufficiency argues designing ambient-energy harvesting systems that trade-off a more efficient design for lower cost but that generate energy sufficient to sustain the monitoring system. Thus, while thermal-to-electric power generation is inefficient, our cost-conscious design (Section 3.2) sufficiently powers our sensing system (Section 5.1). In fact, Section 5.2 shows that

we can go further to *batteryless operation*. Before those experimental results, we next describe our basic TE harvester (Section 3.2), power conditioning (Section 3.3), and the physical mount (Section 3.4).

3.2 Thermo-electric harvester Design

We had several system requirements for our TEG-based power harvesting system to satisfy. First we need a thermo-electric module that works at the 250 ℃ plus temperature typical of the steam injection pipes. Secondly we want the TEG module to harvest *sufficient* energy to directly power mote-class devices. Lastly, we want the power-harvesting module to be low-cost to engender dense deployment.

To satisfy the first two requirement we choose the 1261G-7L31-04CQ thermal power generation module from Custom Thermoelectric [15]. This module has a maximum temperature rating of 260 ℃ and, under ideal conditions, is rated to generate up to 5.9 W. With transmit power at highest gain (+10 dBm) reported to be 82 mW [6] we should have sufficient energy a mote-class device.

We do not use active cooling, or any buffer energy in batteries, to minimize the cost of deployment and maintenance. The cold side of our TE-harvester mates to an aluminum heatsink, measuring $5\frac{3}{8} \times 5\frac{3}{8} \times 1\frac{3}{8}$ inches, While we apply a relatively cheap thermal paste on the cold side, for heat transfer to the heatsink, we did not use any thermal paste on the hot side of the TE-harvester due to its high cost. In Sections 5.1.1 and 5.1.2 we show that our efficiency-cost trade-off in TEG design is sufficient to meet our application needs.

3.3 Power Conditioning the TEG Output

We add power conditioning circuitry to adapt electricity from the energy harvester to voltage and current usable by our sensor node.

For this purpose, we chose the heliomote board designed to power motes using solar power at UCLA [23] for an off-the-shelf solution. Under normal operation, the heliomote board trickle charges 2 NiMH AA batteries from its solar panel input and regulates power to a sensor node.

Given the Heliomote as the power conditioning unit of our system, our first challenge was to adapt it to work with the thermo-electric power. Since electrical property of a typical TEG drastically differs solar panels, simply replacing it with TEG did not work. The heliomote needs an input voltage > 2.4 V to charge the batteries that then supply the energy to be conditioned to mica2. While a solar panel can produce this voltage, a typical TEG generates much lower voltage. We considered charging a single battery at 1.2 V, but some IC's in the heliomote were unable to operate at that voltage. Finally, we configured one of our heliomote unit such that it directly regulates the output voltage of the TEG to 3.0 V. With this modification, the TEG directly powers the mica2 and thus needs to provide all instantaneous power requirements. We verify this capability in Section 5.2.

A final concern is the system behavior during the times when the thermo-electric power is insufficient for our prototype system run properly. (for example, see Section 5.2). To gracefully handle brownout, we enable the brown-out detection on the Atmega128 processor to proactively shutdown if the voltage drops below a user specified threshold.

While our application scenario provides continuously available thermal energy and directly powering our system is acceptable, we are currently also looking into using capacitors (super- or otherwise) to ride any load transients (Section 5.2). We plan to look at modifying existing power regulation circuit designed specifically for thermal power [27] and incorporate design into our thermocouple board.

3.4 Mounting Design

A final step for the deployment of the thermal energy harvesting system is the pipe mounting design. We want a robust and stable design harvesting sufficient energy to power motes. However there were several constraints regarding the pipe mounting.

First, the outside pipe diameters in many oilfields vary between $2\frac{3}{8}$ and $3\frac{1}{2}$ inches. Second, most steam pipes are insulated to prevent heat loss. While we

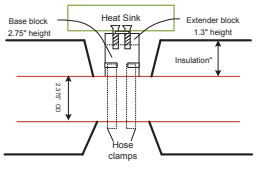

(a) Design of the TEG pipe-mounting apparatus

(b) Deployed mount, without extender block

Figure 4: Mounting design for TEG

have permission to remove the insulation at locations of interest, the insulation thickness varies between 2 to 4 inches at different locations. Since we want the heat sink to be exposed to airflow, we prefer it is located above the surrounding insulation. Third, we wanted a mechanism to securely clamp our system to the heated pipe.

Our solution to the above constraints is shown in Figure 4. The base block of our TEG mounting system is curved to match the exact pipe diameter at our target site ($2\frac{3}{8}$ inches). This base block also has a height of $2\frac{3}{4}$ inches, to allow it to extend past an expected 2 inches of insulation. A separate additional block can be added to accommodate deployment to locations with thicker insulation. Finally, the base block also has curved grooves going through its one side allowing us to pass two hose-clamps on either side and clamp the entire apparatus securely to the pipe.

4 Non-invasive Sensing of Blockages in Pipelines

Our goal is to develop a low cost solution for pipeline blockages detection in steamflooding injection system. The energy harvesting unit (Section 3) reduces the cost to bring power to our system. In this section, we describe how our non-invasive sensing and anomaly detection algorithms reduce the cost of sensing by avoiding piercing of the pipeline. We could network our upstream and downstream sensors, but we did not do that for the ease of prototyping and field-testing.

First, we describe the physics behind steamflood blockages in Section 4.1. Then, in Sections 4.2 and 4.3 we describe our basic detection algorithm and an extended algorithm which has lower false positives.

4.1 Background: pipeline physics

Our hypothesis is that pipe surface temperature can indicate internal choke blockages. In this section we summarize the physics of fluid flow in the pipe to show how a blockage decreases downstream pressure, which in turn decreasing surface temperature, a phenomena we can detect.

To understand what happens in the pipe, we must understand what happens when supersaturated steam passes through the choke (see [34] and [8] for general background). The choke is an intentionally narrow opening in the pipe (a choke *bean*) designed to keep steam at critical flow, where the fluid reaches sonic velocity, effectively isolating pressure upstream and downstream of the choke [8]. This isolation is essential for oilfield operation, since downstream and downhole conditions may vary, and also our algorithm since we can observe temperature differences on upstream and downstream of the choke (T_U and T_D) to detect blockage. As we described in Section 2.2, scaling inside the pipe, steam impurity, and device wear can all cause blockages, which change the cross-sectional size (A) of the choke. We write this change as:

$$A' < A \tag{1}$$

where A' indicates the value after a blockage occurs. The volume of steam passing in a unit time ($\dot{m}$, the *mass flow rate*) is determined by the choke aperture size, so a partial blockage reduces steam volume. The Thornhill-Craver choke rate equation shows mass flow for straight-bore chokes [9]:

$$\dot{m} = 73YA(1 - \frac{0.00625L}{\sqrt{A}})\sqrt{\rho P_U} \tag{2}$$

The flow rate depends on gas expansion factor (Y), aperture size (A), choke length (L), upstream pressure (P_U) and steam density (ρ), calculated by vapor-phase and liquid-phase specific volumes. Field oper-

ations keep ρ constant during normal operation. By the definition of choked flow, P_U is constant as well.

From Equation 2, we see that a partial blockage ($d' < d$) reduces flow rate:

$$\dot{m}' < \dot{m} \tag{3}$$

Since steam is compressible, a decrease in mass flow decreases pressure [34]:

$$P'_D < P_D \tag{4}$$

A lower downstream pressure reduces internal steam temperature ($T_{D,i}$) and therefore pipe surface temperature. Experimental data shows this relationship with internal temperature [13], as shown by the the following empirical equation provided by field engineering:

$$T_{D,i} = \frac{7006.3}{9.48654 - \ln \frac{P_D}{144.9}} - 382.55 \tag{5}$$

Since we know that surface temperatures follow internal temperatures ($T_D \propto T_{D,i}$), drop in pressure implies drop in temperature:

$$T'_D < T_D \tag{6}$$

and upstream temperature and pressure are not changed ($T'_U \approx T_U$, because it is choked flow),
so we can therefore detect blockage by looking for relative temperature differences:

$$T'_U - T'_D > T_U - T_D \tag{7}$$

The above reasoning suggests why choke blockage is visible in our system. However, oilfields are complex, and choke blockage is not the *only* possible cause of pipe temperature changes. Weather changes on the surface, and downhole pressure changes are both potential sources noise. Our detection algorithm (Section 4.2) triggers on *sudden* and *relative* temperature differences, so it should not trigger on surface changes that affect both sensors (such as weather, since the relative differences between the sensors are unchanged), or gradual downhole changes (such as reservoir changes, since they take place over days or weeks).

In this section we summarized how blockage eventually reduces downstream pipe skin temperature and we provide theoretical and empirical equations to prove that. Griston *et. al.* observes similar phenomenon that smaller choke bean size does not affect upstream temperature much while significantly reduces downstream temperature in their experiments [13]. These results are consistent to our hypothesis that we can use temperature to detect choke blockage remotely. This background is used in our algorithm design to provide good detection accuracy (Section 5.5).

4.2 Design of the base algorithm

We next apply our observation that pipe temperature relates to flow rate to detect choke blockage (Section 2.2). Since blockages represent changes in flow behavior, the principle of our algorithm is to look for changes in temperature *upstream and downstream* of a possible point of blockage, and to comparing *short- and long-term* temperature averages. Our algorithm adaptively learns the temperature model of a normal pipe from long-term history. The short-term history filters out noise while detecting rapid changes in pipe temperature that indicate blockage events.

We study two kinds of blockages, each with its own inference derived from Section 4.1:

partial blockage The pressure before the blockage site remains relatively constant since it is part of the large steam network and some steam still flows through the choke. However, downstream from the choke pressure decreases because of a smaller effective orifice size. Therefore a large drop in downstream temperature relative to upstream indicates a partial blockage.

total blockage Downstream of block, steam stops flowing, so pressure and temperature immediately drop, and eventually it converges to ambient temperature. Upstream temperature also drops because steam cannot flow through the pipe, although because upstream remains connected to the steam network it may remain higher than ambient temperature.

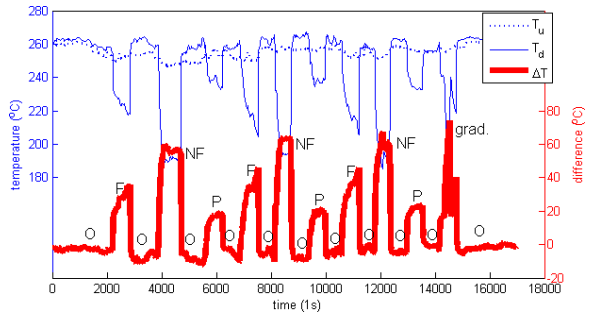

Figure 5: up/down-stream temperature and ΔT fluctuation upon different blockages. Letters on the graph show approximate status of the valve simulating blockage: F: full blockage, NF: for nearly full, P: partial, and O for valve open (no blockage).

We show experimental results validating this hypothesis in Figure 5, with letters indicating degree of emulated blockage. (Definition of blockage levels in our experimental system are in Section 5.4.) We see that upstream temperature is relatively stable, although it dips slightly upon full and nearly full blockage. Down-stream one is much more sensitive to pipe status and hence we observe 10 distinct temperature differential (ΔT) peaks for 10 blockages ($3 \times 3 + 1$) respectively. We evaluate our base algorithm in Section 5.4 to test under various blockage.

We show the algorithm pseudo-code in Algorithm 1. We first compute the short- ($s(\Delta T)$) and long-term ($l(\Delta T)$) history of the difference between upstream (T_u) and downstream(T_d) temperature via exponential weighted moving average. We choose EWMA because it is light weight and easy to implement our 8-bit mote platform; short- and long-term EWMAs may use separate gains (α_s and α_l). Whenever the difference (δ) between two history exceed pre-defined threshold (th_block), the system declares pipe blockage.

After a blockage is detected, we expect responders to investigate the problem and reset the algorithm after it is corrected. Since in our field tests (Section 5.4) we artificially induce blockages rapidly (in tens of minutes), we employ two addition rules for rapid testing. One is that after blockage detected, when two history series converge ($\delta = 0$), we automatically reset pipe state in order to precede to follow-up tests. The other is that we stop updating the long-term history when the pipe is in anomaly state (i.e. any non-normal state). These rules allow our short-term tests to mimic long-term operation with response teams.

Our algorithm successfully detects pipe clog at choke, as shown experimentally in Section 5.4. Although this algorithm is correct, upstream maintenance can cause false alarms because they too cause pressure drops. The next section shows an improvement to avoid these false alarms.

Algorithm 1 Blockage detection algorithm.

Require: $T_u, T_d, th\_block, th\_maint, th\_norm, \alpha_s$ and α_l.
Ensure: Pipe state s.

```
1:  s ← NORMAL
2:  while system on do
3:    ΔT ← T_u − T_d
4:    s(ΔT) ← s(ΔT) + α_s × (s(ΔT) − ΔT)
5:    l(ΔT) ← l(ΔT) + α_l × (l(ΔT) − ΔT)
6:    δ ← s(ΔT) − l(ΔT)
7:    if (δ ≥ th_block) ∧ (s = NORMAL) then
8:      s ← BLOCKAGE
9:      print "Pipe blocked"
        {*** below are extensions from Section 4.3.}
10:   else if (δ ≤ th_maint)∧(s = NORMAL) then
11:     s ← MAINTENANCE
12:   else if (δ ≥ th_norm) ∧ (s = MAINTENANCE) then
13:     s ← STABILIZATION
14:     start timer
15:   else if (timer fired) ∧(s = STABILIZATION) then
16:     s ← NORMAL
17:   end if
18: end while
```

4.3 Avoiding false positives

The above algorithm detects blockages around the target, but regular steam distribution maintenance will also change system pressure and temperature.

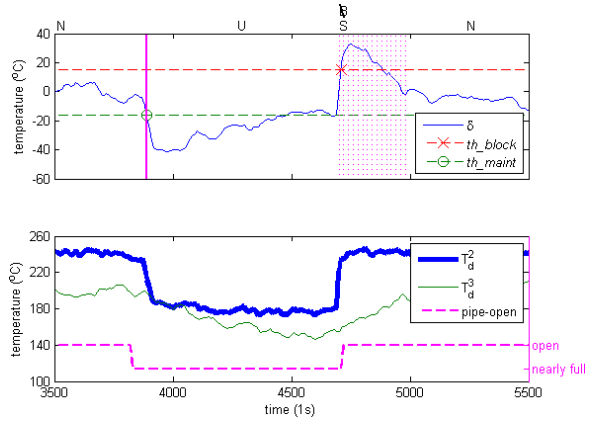

Figure 6: The cause of false positives and our solution. *N, U* or *S* means the pipe is in *normal* , *upstream maintenance* or *stabilization* state respectively. A slashed-out *B* shows a false blockage detection suppressed.

Our base algorithm is unable to distinguish maintenance from choke blockage, thus incurring false positives. We can avoid false positives by employing networked sensor readings from other parts of the steam distribution system. We next describe how we extend our base detection algorithm to distinguish system-wide changes from local blockages.

The lower plot of Figure 6 excerpts a particular false alarm example and illustrates how our extension works. We distinguish upstream maintenance from blockage by detecting the both start and stop of maintenance period. We decide maintenance start if $\delta < 0$ because of the inertia at the choke making the upstream temperature drop before the downstream (time $\approx$ 3800s). Likewise, we detect the stop at the next $\delta > 0$ since the same inertia causes a reverse process (time $\approx$ 4700s). Our extended algorithm then gives the pipe a stabilization time period and suppresses any following potential δ peak, which the base one would misinterpret as blockage (the cross marker at 4710s). We detect blockage by any δ that larger than *th_block* but falls out of the stabilization period (i.e. not preceded by a sign of maintenance start).

We discussed how we extend our base algorithm to avoid false positives. The evaluation in Section 5.5 shows it successfully distinguish upstream maintenance from blockage. We then discuss the method of parameter tuning in the next section and shows our algorithm is generic to applications other than steam pipe.

4.4 Tuning for different environments

We developed the algorithm to detect steampipe blockages, but will also show in Section 5.6 that, with proper tuning, the same algorithm applies to hot water distribution networks. We next show how to tune parameters to work in either case.

The detection thresholds (*th_block*, *th_maint* and *th_norm*) are critical to trade-off accuracy, responsiveness and reliability. We assume ΔT follows a normal distribution $N(\mu, \sigma^2)$. Usually *th_block* is set higher than 3σ, according to 3-sigma rule [11]. The water in PVC pipe has lower temperature and hence we observe less significant ΔT variance upon anomaly. To make accurate detection, we set both *th_block* and *th_maint* closer to 0. *th_norm* could be simply configured to a small enough value to ensure hysteresis in our algorithm and we by default set it to 0.

Short and long-term gain (α_s and α_l) determine how our algorithm reacts to noise and how fast it could response to blockage. Long-term history should be relatively stable while short-term agile. Pipe material (metal vs. PVC) fluid type (steam vs. water) or ambient environment all affect how quick the temperature reacts to pipe status change. With PVC and water, the pipe material has better heat insulation than metal, and hence we want to keep long-term history more stable because of the sluggish short-term change. Observing the forgoing rule, we propose that $1/2$ for short-term EWMA gain and $1/64$ for long-term in steam application while $1/4096$ in water one.

Finally, the stabilization time period helps avoid false positives. We find that a 360s timer is enough for suppressing most noisy jitter when upstream maintenance done. The reason is that it takes δ about 950s to subsides, with α_l of $1/64$ and the peak usually happens within the first half of the period. For water pipe, since we are using smaller α_l and non-metal

pipe, we set a longer timer because it takes accordingly longer to stabilize.

5 Evaluation

This section describes the methods of evaluation and their results for our problem detection system. We begin by considering energy harvesting: how much energy does it require and can steam-power provide (Section 5.1) and whether we can operate our sensor nodes without batteries (Section 5.2). In terms of sensing, we consider sensor accuracy and calibration (Section 5.3). Finally, we show that the algorithm also applies to lower-temperature water pipelines (Section 5.6) and that it works in the field (Section 5.7) at much lower cost than today's systems (Section 5.8).

5.1 Long-term harvesting and consumption potential

The steam-power system requires two things, sensor nodes that are able to sense temperatures and execute the blockage detection algorithm and energy harvesters that are capable of producing sufficient electricity for their corresponding sensor node. To evaluate this, we next look at both TEG energy generation as a function of temperature difference and load, and the energy consumption of our application. We show that there is ample energy available for harvesting to drive a mote-class sensing system, even with relatively small temperature differentials.

We first describe the result of experiments validating the energy harvesting potential of our TEG sandwich at two location: in-lab and on-site.

5.1.1 Energy Production: In-Lab Prototype

We simulate steam-pipes using a laboratory hotplate (Thermolyne Type 900). This rectangular hotplate can be heated up to the desired 260 ℃. For our lab prototype, we used a small "hot"-block, 0.5 in high and about the size of the TEG itself, for the contact between the TEG hot-side and the hotplate. The close proximity of the hotplate (with a larger surface area than the hot-block) , however, results in a hotter heat-sink due to heat convection. Thus the thermal differential across the TEG actually starts to fall with time and the TEG produces little power. A similar observation has been made in a separate previous work [41].

In order to simulate an expected temperature differential of 80-100 ℃, we made two changes to our setup. First, we increased the height of the column supporting the TEG sandwich (consisting of the heat-sink, TEG, and the hot-side mount) to around 1.5 inches above the hotplate (Figure 7(a)). Increasing the distance from the heat source, paradoxically, results in better energy generation due to lesser heat convection from the hot-plate. We also use a small fan to simulate breeze to maintain a low equilibrium temperature at the heat-sink.

With a test harness providing a stable temperature differential, we next observe the voltage, current and power characteristics of our TEG sandwich. We built a high wattage resistor network, where we can vary the load and measure voltage to infer power (Figure 7(a)). An ammeter was not used as the range of current sourced by the TEG varies between 3 mA to 800 mA and requires switching the Ammeter contacts in between this range.

We measured the characteristics of the TEG at different temperature differential across the TEG. Figure 7(b) shows power characteristics of our prototype TEG sandwich in lab. We observe that under most operational conditions (temperature and load), our prototype can provide greater than the approximately 100 mW needed to power mote-class devices [6].

5.1.2 Energy Production: on-site

Our final TEG mounting design is significantly different from the prototype (details in Section 3.4) to allow fitting on the steam-pipes. Moreover the ambient temperature at our intended deployment locations reaching 50 ℃ in summers.

To verify that our deployment version also harvests sufficient energy we visited an operational oilfield of our partners and deployed the TEG mounting appa-

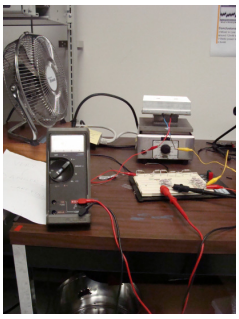

(a) TEG power measurement harness: hotplate, cooling fan, and the resistor network (load) shown here.

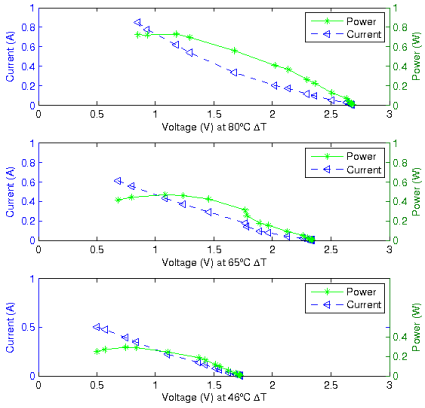

(b) TEG power curves at different temperature differentials. For even a 46 ℃ differential, the TEG can output > 80 mW.

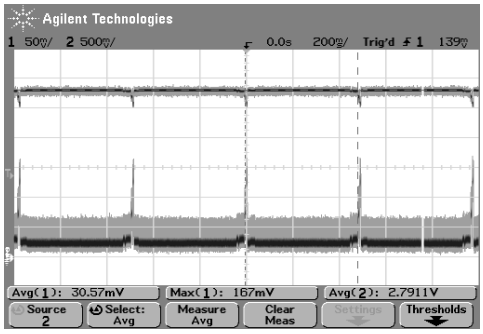

(c) Periodic sampling application: The top line (channel. 2) shows voltage of TEG and the bottom line is voltage across a 1.2Ω resistor (for current measurement).

Figure 7: Setup for Power measurement and results: With optimal loads and depending on temperature differential, TEG can provide between 0.3-0.8 W. The average power consumption of our steam-sensing application, meanwhile, is ≈70 mW.

ratus on an steam pipe in December 2009. With our sensing platform still under development, we simply logged the open-circuit voltage of our TEG and spot-measured the temperature. We observed a nearly constant temperature differential of 100 ℃ and open source voltage of 3.8 V. Our measurement result from a three hour deployment verify that our pipe-mount TEG can harvests energy comparable, if not greater, than the lab prototype. They also confirm, consistent with theory, that power generation increases both with temperature differences and higher absolute temperatures. We now compare this harvested energy with the energy consumption of our blockage detection system.

5.1.3 Energy Consumption of Sensing

Our steam-sensing systems employs mica2, with power regulation using a modified heliomote board and a custom amplifier board to interface with thermocouples. The entire system, therefore has additional components beyond the mica2 for which their are published energy consumptions results [6]. We therefore measured the power draw of our system running the blockage detection algorithm (Section 4.2). by adding observing the voltage drop across a 1.2Ω resistor in series with our TEG and the load.

Figure 7(c) shows the consumption profile featuring periodic sampling of temperature. We observed an average current drawn of 25 mA and an average voltage output from TEG of 2.8 V. Hence the long-term power consumption is 70 mW, close to the highest power transmission of 80 mW reported for mica2 here [6].

The above result, coupled with the power harvesting results in previous sections show that our TEG can harvest significantly greater energy than needed to meet the long term requirements of our sensing system.

5.2 Batteryless operation?

While Section 5.1 shows there is ample available energy to operate our sensing system, our system eliminates the battery completely (Section 3.3) to directly power it. For such batteryless operation, energy

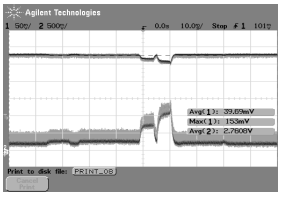

(a) Logging to flash (erase-write) causes two load spikes.

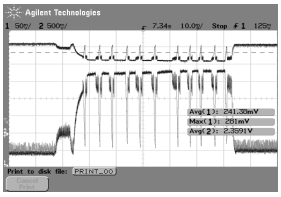

(b) At temperature differential below 80 ℃ these spikes cause failure and result in a reboot.

Figure 8: Instantaneous load can cause failure.

Table 1: Energy buffering test at TEG $\delta T = 83.1$ ℃

Add-on capacitor (μF)	**System operation status**
No capacitor	always reboots upon logging
1000	logs 2 packets before rebooting
3300	logs 12 packets before rebooting
4300	no rebooting and works fine
6600	no rebooting and works fine
9900	no rebooting and works fine

harvesting must not only meet the average energy demands over long-term but also the *instantaneous power* requirements during continuous operation.

Given the large amount of headroom we showed previously, we expected that batteryless operation would be straightforward. Unfortunately, we found that writing to flash has a high short-term power draw. Figure 8(a) shows the erase-write spike typical when writing to flash. These instantaneous spikes consume, at their peak, around 0.26 W.Using the hotplate and fan to create a temperature differential across our TEG sandwich, we observed that when this difference drops below $\approx$ 80 ℃[1] the mote rebooted (Figure 8). We conclude that tasks with large short-term power draw make batteryless operation difficult. In our case, we chose to disable flash logging in favor of logging to the network.

An alternate approach is to temporarily buffer energy in a capacitor after the power regulation by heliomote. This approach avoids use of a chemical battery, but the capacitor provides some ability to tolerate bursty energy requirements that occur during flash write due to data logging. In order to test whether capacitor covers peak energy usage, we carry out a two-step test. First, we want to know if our system can work under a lower TEG power output. Using the hot-plate based test harness (described in previous section) we observe that our sensing system (mica2, heliomote, amplifier board, and thermocouple) needs a baseline of 50 ℃ TEG temperature differential (δT) to simply turn on. We add a 1000 μF (to store the 2.3 mJ of energy needed for the spikes) capacitor and observe that, with logging enabled, the system now reboots around a δT of 60 ℃. Thus, including a capacitor allows us to log with just 20% higher operational δT from the baseline; however without any capacitor we need 60% higher operational δT.

Knowing a capacitor with moderate capacity (1000 μF) do help reduce the system operational TEG δT, we proceed to the next step – whether capacitor capacity matters. Table 1 shows the correlation between capacitor and system robustness. In general as we expected, bigger capacitor buffers more energy and hence logging fails less frequently as TEG output power fluctuating (mainly because of hotplate temperature oscillation). We here assume the charging time for capacitor with any capacity is always sufficient, since our current scan interval is 10s while it takes only tens of milliseconds to fully charge a 3000 μF capacitor in our system. In all, we conclude that a large enough capacitor do improve our system robustness.

5.3 Can we measure temperature accurately?

The premise of non-invasive sensing is that pipe surface temperatures are able to predict blocking and constriction inside the pipe, and that we can evaluate pipe surface temperature reasonably accurately. We next evaluate this claims, examining how we calibrate temperature sensing in spite of several potential sources of observation error. We breakdown the cal-

[1] temperature difference measurement is imprecise with +/- 5 ℃ range due to variable contact using a manual thermocouple

ibration into following steps, from pipe raw temperature to thermocouple output, to mote input value and finally to mote ADC readings. We show that our system is accurate enough in each steps to detect problems without careful calibration, but that with calibration we can predict internal temperature accurately enough to infer internal flow rates given a known fluid.

The first step of calibration is from pipe temperature to thermocouple with two major factors. One is the pipe insulation because it significantly affects measured temperature distribution (μ and σ). To mount thermocouple on pipe, we have to temporarily tear down the insulation material, usually thermal sponge and aluminum wrap. We test temperature collected before and after insulation re-apply from the same sensor and we find that mean temperature rise from 244.86 ℃ to 265.37 ℃ and σ drops from 3.00 ℃ to 0.78 ℃, with all other condition remaining the same. In other words, we observe less environmental noise and closer to steam temperature, if pipe properly insulated. The other is thermocouple-to-pipe contact. We believe hose-clamp style provide firmest contact than other styles, say magnet or general-purpose (stick) probe. In the field, we observe that our hand-held Sper Scientific thermometer with general-purpose probe could not measure repeatable temperature, mainly because of the pipe curvy and rusty surface.

Another calibration concern is thermocouple voltage-to-temperature (V-T) non-linearity. We want to know whether V-T relation approximates linear in a small temperature range, since in the entire space, usually we have to use high order polynomial conversion [36]. From J type thermocouple calibration reference table [12], we pick up all points of which temperature ranges between [0, 310] ℃. We then use linear fitting find the gradient for V-T relation is 18.259 and the y-intercept is 2.852. The R-squared value of the fitting is 0.99995 and the standard deviation of error between look-up table and fitting points is 0.887 ℃. This shows the V-T relation is linear enough for our algorithm.

The second step is from thermocouple output to mote input voltage. We find that to run our detection algorithm, it is unnecessary to do the calibration. According to Seebeck effect, a voltage potential at the two ends of a conductor when a temperature gradient could be established along it [36]. When two different material soldered at one point, we measure its temperature gradient by the voltage difference between two legs of the custom thermocouple. We need the reference point temperature (T_r) to calibrate each thermocouple because of the thermocouple-to-voltmeter connection. However, we are more interested in the reading difference between two thermocouples than individual accurate reading. Hence, no T_r calibration is required here because we find the reference junction errors from two thermocouples cancel each other if both in the same isothermal box.

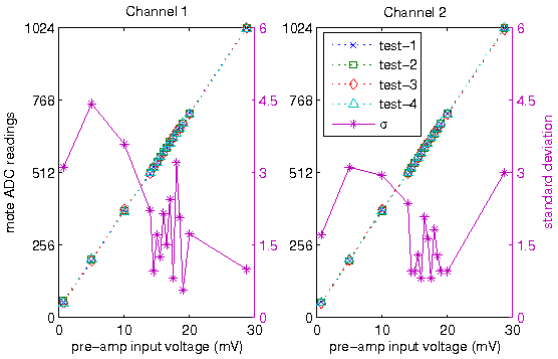

Figure 9: Amplifier board repeatability test result.

The last step is mote input voltage to mote ADC value. There is one last variable in this step, our custom amplifier board. We first verify the two op-amp channels connected to thermocouples behaves the same. We connect thermocouples, amplifier board and mica2, feed the same voltages to both op-amp channel and record ADC values returned from mica2. We sample different voltages and repeat the test for four times. We report test result from one of the amplifier boards since they are fairly close. The mean difference between two channel is 1.17 and σ is 0.68. Next we quantitatively test the board repeatability (Figure 9). From the four test, we conclude the two channels are stable enough.

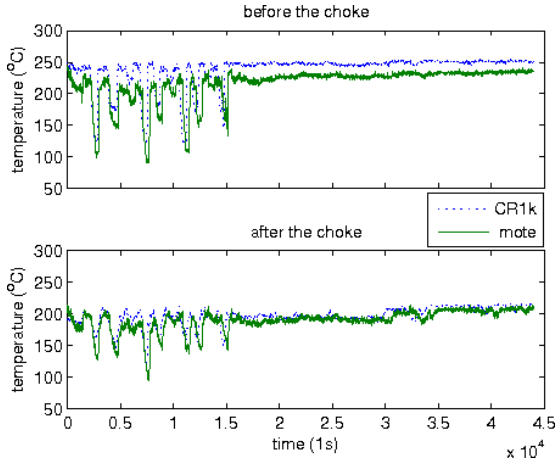

Figure 10: temperature measured by mote and CR1k.

$$T = 18.259 \times \frac{ADC \times 3 \times 1000}{2^{10} \times \beta} + 2.852 \qquad (8)$$

Finally, we combine and test all calibration steps. Figure 10 shows that if we direct convert ADC to temperature with minimum calibration, according to Equation 8, we would only have near constant error for each channel. V is voltage in mV and $\beta = 100$ for the amplifier board gain. This clearly proves that we can run our detection algorithm directly over ADC value returned by mica2.

In all, we draw 2 conclusions. One is that our system is linear enough to run our algorithm without calibration. The other is that with post-facto calibration we can predict temperature accurately. Further, according to Equation 5,we believe accurate pipe skin temperature eventually helps us estimate in-pipe pressure and steam flow rate.

5.4 Does our detection algorithm work?

Given our inexpensive, fully wireless platform, our next step is to show we can detect problems. We expect our base algorithm to work on all kinds of blockage level: full, nearly full and partial.

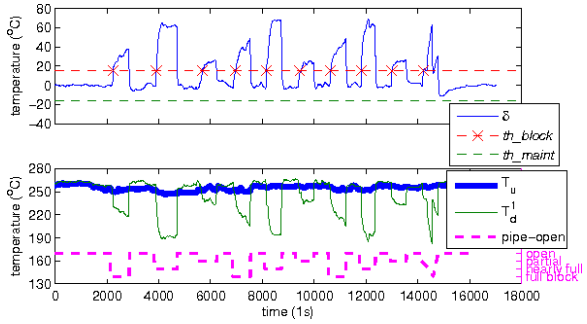

Figure 11: Similar base and extended algorithm result on the sensor pair straddling the valve with $th\_block = 15, th\_maint = -16$, $\alpha_s = 1/2$ and $\alpha_l = 1/64$. The bottom plot shows the raw up- and down-stream temperature with pipe status mapping.

Since it is difficult to simulate blockage by choke, we alternatively use valve on steam pipe to carry out our experiment. Field engineers helped us to toggle the valve between fully blocked (flow rate $\dot{m} = 0$), open ($\dot{m} = 100\%$) , nearly fully blocked ($\dot{m} \approx 10\%$), open, partially blocked ($\dot{m} \approx 50\%$) and open again. We repeated the procedure three times and finally, we slowly but continuously shut off the pipe within 9 min to observe a gradual blockage. The dash line in the bottom plot of Figure 11 depicts the whole procedure. We deployed Campbell Scientific CR1k datalogger with NANMAC D60 hose-clamp thermocouple and collected more than 12-hour long temperature trace (1pm Mar 4^{th} through 1am Mar 5^{th}). Figure 2(a) shows our sensor placement.

Figure 11 presents the result of our base algorithm with $th\_block = 15$ ℃. The top plot clearly shows how δ peaks triggers detection under our threshold setting and the bottom plot provides the raw up- and down-stream temperature data mapped to pipe status change. Short- and long-term EWMA gain are fixed to $1/2$ and $1/64$ respectively for this analysis according to Section 4.4. We have examined choices of both long- and short-term gain (evaluation omitted due to space) and believe that these parameters are suitable for our application.

A general observation is that our algorithm correctly detects *all* of the blockages (we ignore the final

gradual blockage in the following evaluation). All 3 level blockages yield δ peaks higher than 15 ℃ and are captured by our system. If we examine the bottom plot of Figure 11 more carefully, we find that, first, as we expected, up-stream temperature is relatively stable under all kinds of blockages, although slight drop upon full and nearly full ones. Down-stream one is much more sensitive to pipe status and hence we observe ten distinct peaks for ten blockages ($3 \times 3 + 1$) respectively. Second, surprisingly, that nearly fully blockage yield the most down-stream temperature drops and corresponding up/down difference, even more than complete cases. And the top three δ peaks belong to this type of blockage. We believe that this is caused by *choke flash* – when the valve is closed small enough it starts choking fluid. On the contrary, total blockage completely shut-off the flow and occupies downstream side pipe with "back" pressure from reservoir through injection well, according to field engineer. Third, partial blockage is the hardest to detect. Insignificant downstream temperature drop constrains our *th_block* selection. Fourth, our algorithm is highly responsive. For example, it takes averagely around 6 samples (60s) to correctly detect problems when $th\_block = 15$. Larger *th_block* may affect the detection delay, but not too much. Finally, carelessly configured parameter would trigger false alarms. An over-aggressive *th_block* value (≤ 5 ℃) mistakes normal temperature fluctuation for pipe anomaly. However, one could easily avoid the problem by taking temperature intrinsic property in account, e.g. mean and deviation.

In all, we conclude that our base algorithm is capable of detecting all 3 kinds of blockage, especially nearly full and full easily. According to the field engineer, partial blockage is exceptionally rare in real field. However, when we run our algorithm over the sensor pair straddling the choke, our base algorithm triggers false alarms as we discussed in Section 4.3. The same blockage threshold captures seven out of ten positive δ peaks in Figure 12. We next evaluate our extended algorithms for avoiding false positives.

5.5 Can we avoid false positives

Section 5.4 shows that our base algorithm has good accuracy on target choke blockage detection. However, it fails under the second scenario, MAINTENANCE and triggers false alarms, which we show and discuss later. In order to distinguish both scenarios, we proposed extension to our base algorithm in Section 4.3. In this section, We evaluate the extended algorithm over the valve-straddling sensor pair (T_u and T_d^1) first and then the choke-straddling pair (T_d^2 and T_d^3). We expect the extension should work on both scenario, i.e. successfully detect target blockage and MAINTENANCE while suppress the false positives at the end MAINTENANCE state.

For the same threshold and EWMA gains, the extended algorithm yields exactly the same result as that of the base one over valve-straddling pair for target choke blockage detection (Figure 11). *th_block* still successfully captures all blockages while *th_maint* triggers no false alarms. In short, we prove that the extensions does not impair our base algorithm performance.

We then evaluate how the extended algorithm avoids false positives over the second sensor pair and Figure 12 shows the result. As we discussed in Section 4.3, each upstream valve operation incurs a positive δ peak after a δ valley because of the asynchronous temperature drop on both sides. The base algorithm with same threshold as we used in the first sensor pair evaluation ($th\_block = 15$) captures seven out of ten positive δ peaks upon up-stream valve operation, although the actual choke remains open all the time. However, the extended version triggers *no* false alarms any more (seven slashed-out "B" tags). The stabilization period (dotted stripes tagged as "S" in the top plot) successfully suppress all positive δ peaks as soon as MAINTENANCE anomalies are reset and δ rises back above 0. Besides, the system with *th_maint* detects all ten MAINTENANCE events (tagged as "U"). Contrary to target valve blockage scenario, fully up-stream blockage is the easiest to detect. The reason is that the sensor pair is deployed far downstream to the blockage spot (the valve) and the choke effect subsides. Fully blocked pipe has no flow while heat is still near-constantly dissipating, creat-

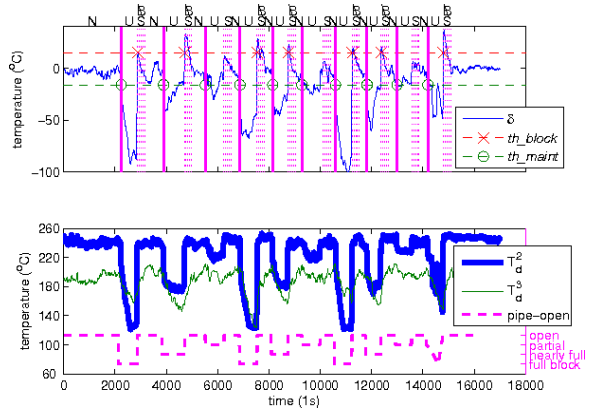

Figure 12: Extended algorithm result on the sensor pair straddling the choke with $th\_block = 15$, $th\_maint = -16$, $\alpha_s = 1/2$ and $\alpha_l = 1/64$. The bottom figure shows the raw up- and down-stream temperature with pipe status mapping.

ing the largest ΔT drop.

We carefully evaluate our improved algorithm in two different scenarios — target blockage and upstream maintenance with temperature data straddling the valve and the choke. We demonstrate that our extended algorithm yields good accuracy and triggers minimum false alarms. We next considers applying our generic algorithm to other applications.

5.6 Generalizing to other applications: low-temperature, incompressible fluid

We have shown our approach works for applications in steamflood fields. We further believe our general approach of non-invasive sensing can apply to other kinds of pipelines. However, the physics of what is being distributed affect the sensing: steam is a high-temperature, high-pressure, compressible mix of water vapor and fluid. Water has very different physical properties: most importantly it is incompressible, as well as lower pressure and temperature. These difference make detection of partial blockages difficult, but we next show that we can still detect full blockage in hot water distribution networks.

Figure 13 shows our testbed prototype and sensor placement schema. Our hypothesis is that we should detect both partial and total pipe blockage by our algorithm in Section 4, with a different parameter set from oilfield. It is composed of a tankless water heater, a hot water recirculation pump, a plastic lidless tank, PVC pipes and valve fittings. During the 7-hour long experiment, we used Go!Temp USB-based temperature sensors [16] to collect pipe skin, ambient and reservoir water temperature and different levels of blockage are simulated by manual valve control. For example, we turned valve on artery line $n\%$ off and leave other branch pipes 100% open to mock up a $n\%$ partial blockage.

Figure 14 shows how up- and down-stream pipe temperature changes and Figure 15 gives detailed aggregated temperature history and difference. The sampling rate is 1 Hz and we set short- and long-term EWMA gain to $1/2$ and $1/4096$ respectively. Table 2 lists our procedure and compares median temperature upon different pipe status. The first observation is that large downstream temperature drop occurs upon total blockage. Temperature decrease from about 44 ℃ (dot-shadowed region in both figures) and finally converges to 39 ℃ in about 1,500s. As soon as the pipe status is back to normal, downstream temperature restores to 44 ℃ immediately (about 300s). The second observation is somewhat surprising. Unlike that of total blockage, the temperature change upon partial blockage (2040s–4914s and 14790s–23314s) is insignificant, except upon near-total (90%) blockage at the end of the experiment. Third, we find that contrary to downstream temperature, the upstream temperature remains relatively stable all the time. It is expected because, according to the placement schema in Figure 13, the upstream sensor is before the branch point, and hence regardless the artery pipe status, fluid always flow undisturbed at least through the branch pipe.

From above observations, we reach raw following conclusions. First, our algorithm successfully detect total blockage (or near-total) in low temperature, low pressure and incompressible fluid pipe. When flow in pipe stops, although some fluid still trapped in it, the downstream pipe eventually converges to ambient temperature as steam pipe. Figure 15 shows that

Table 2: Experiment procedure and results

Time (s) start	Time (s) end	Pipe status	Median up/down ΔT (℃)
0	2039	Normal	2.7
2040	4914	50% blockage	3.1
4915	10074	**total** blockage	8.2
10075	14789	Normal	3.0
14790	16394	25% blockage	2.7
16395	18199	50% blockage	2.7
18200	19814	60% blockage	2.7
19815	21569	70% blockage	2.7
21570	23314	80% blockage	2.7
23315	25199	90% blockage	7.0

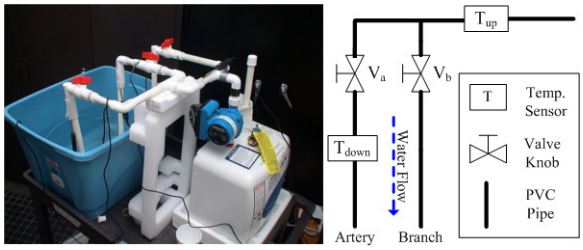

Figure 13: In-lab water-based pipeline prototype.

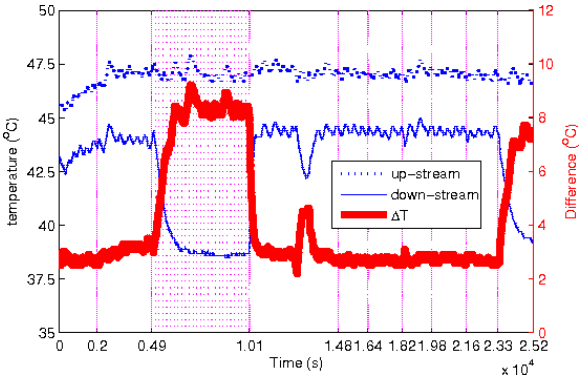

Figure 14: Up/down-stream temperature and difference in water-based experiment.

the difference of short- against long-term temperature history (ΔT) rises significantly from 0 ℃ to a peak of 5 ℃. And a threshold could be easily set to detect the pipe status change. Second, it is difficult to detect partial blockage on our water-based testbed, contrary to steam distribution pipe. The main reason is that water is incompressible, and hence partial blockage has only insignificant influence on fluid pressure as well as temperature. We expect different flow-rate, velocity and pressure fluctuation responding to partial blockage for steam. Another reason is that PVC pipe buffers more heat and dissipate slower than copper pipe.

5.7 Evaluation of complete sensing system

We have conducted several field experiments that were designed to evaluate, develop, and verify three

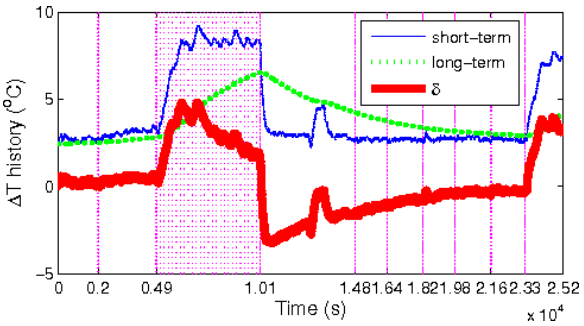

Figure 15: Short/long-term history difference in water-based experiment

.

aspects of the overall system operation: (1) sufficiency of the thermal electrical generator for modified mote class systems, (2) effectiveness of the steam-flood choke blockage detection algorithm, and (3) robust operation of the complete system in the operational oil field. Our experiments included iterative in-laboratory experiments followed by a number of oil field trips to Bakersfield, California.

For our prototype hardware design, we surveyed and obtained a number of inexpensive commodity components. In the laboratory, we conducted controlled experiments on TEGs on a hot plate to collect range of generated power. Based on our measurements and survey of the mote class system, we determined that the electricity generated by our prototype would be sufficient under a typical condition at the oil field. Then we made some simple modifications to the Helimote and Mica2 and successfully operated the sensor node with electricity generated by the TEG placed on the hot plate at lower than expected temperature. Through this experiment, we verified in the laboratory that our TEG system will be sufficient to power the prototype node.

As a parallel effort, we designed a generic blockage detection algorithm based on a simple principles of thermodynamics. Due to non-trivial access to the actual steam pipelines in field, we designed our algorithm to be parametrized and easily tunable. As a precursor to our field experiment, we also built a scaled down version of a hot water pipeline to test our algorithm. Using the experimental results on the testbed, we were able to tune the parameters to effectively detect water pipeline blockage in the laboratory.

During this time, we visited Bakersfield steam-flood oil field to make the initial measurements on the pipelines. We instrumented the steam pipelines with the thermocouples and TEG and collected the changes in temperature and generated power with a datalogger. Using the steam valve, we also emulated the blockage conditions by opening and closing the valves over different durations. The data was analyzed to make tune the parameters of our algorithm. Based on the range of temperature seen in the actual data set, we designed a custom amplifier board and connected range specific commodity thermocouples to measure temperature information at a sufficient resolution without causing damage to the prototype.

Then, two set of prototype systems were transported to Bakersfield for more complete system operation experiments. The prototype system was programmed to run our algorithm as well as take logs of all the measurements. For this experiment, we instrumented our prototype around the steam pipe valves and the choke. As in the previous in-field experiment, we emulated the choke blockage by closing the valves. During this time, results of the algorithm and temperature data were transmitted wirelessly and recorded on a laptop. Although secondary battery was connected to the laptop, its limited battery life cause the laptop to fail sometime in the middle of the night. However, data collected during the day proved to be sufficient and we verified that our batteryless prototype did not reboot and continued to transmit correct measurement data by reconnecting the laptop to the system in the following morning.

In addition to the logging difficulties, we found that the data collected by the sensor node around the valve was not correct due to electrical coupling of the thermocouple sensors. Therefore, we could not confirm the correct workings of algorithm in the field. However, the ground-truth temperature sensors were instrumented right next to these thermocouples and successfully recorded all the data. In the laboratory, we were able to adjust the parameters to the algorithm and verify the correct response of the system using the recorded data.

5.8 System cost

Our claim is that our shift to small, non-invasive sensors driven by harvested power can significantly reproduce deployment costs. To evaluate this claim, we next compare typical deployments today with cost estimates for our system.

Currently deployed systems: Figure 16 shows as a current invasive pressure sensor: the circular pipe fitting in the left of the figure with two large protruding taps. Installing a tap costs several thousand dollars (mostly due to skilled labor) and requires shutting down that portion of the steam pipe. Installation

Figure 16: Invasive flow sensing with solar panel for power.

costs of pressure sensing points and power to the sensor can be as high as US$20,000 per site. Not shown is the sensor itself, a device costing several thousand dollars that takes differential pressure readings from these taps. The figure does show the large (about 30×30 cm) solar panel and car-sized battery needed to support this traditional, power-hungry sensor. According to the field engineers, the estimated cost of the pressure sensors, a datalogger, and a solar panel based battery packs is from US$5000 to US$10,000.

Because of these expenses, a great deal of sensing in oilfields remains human-centric. Because of the high cost of installation, not all the steam injection sites are equipped with the monitoring points. Due to high cost of the sensors, sensors are often moved from one site to another manually. Accordingly, a field technician visits the site about once a month, attaches sensors and a datalogger to the sensing point to records pressure data over some duration, and uploads this to the field SCADA system via a laptop computer. This task requires at least three person-hours per test sites. Such human-driven sensing reduces deployment costs, since the sensing points are installed when the line is built and the cost of the pressure sensor is amortized over many measurement points. Human-in-the-loop makes the operational cost of each measurement fairly high when labor, equipment, and travel time are considered: easily hundreds of dollars per measurement. This high cost for each measurement discourages frequent measurements and so prevents easy detection of problems before they occur. In addition, we expect this recurring cost to rise in future years as the workforce ages and so the cost of human monitoring rises.

Our sensor-network-based system: By comparison, the capital cost of our system is quite modest. Our prototype unit consists of a Mica2 (US$100) for control, a modified heliomote (US$125) for power conditioning, a custom amplifier board (US$50) and two thermocouple sensors (US$70 in total) for sensing, the TEG (US$50) and a custom heatsink and mount assembly (US$200). Despite the system being a research prototype and so not benefiting from economies of scale, component costs are less than US$600. We expect these costs would be reduced in volume.

More importantly, both the deployment and operational costs of our system are quite low. Deployment can be done by a technician in an hour or two (deployment time for our field experiment was 2 hours, and we expect future deployments to be half that). Since deployment is non-invasive, steam flow need not be interrupted and new plumbing is not required; since it is self-powered, electrical expertise is not required. The primary technical skills are SCADA integration and skills for working safely around high temperature pipes. We estimate deployment cost at around US$300.

We see *no* recurring operational costs for sensing.

We believe these significant reductions in both acquisition and operation will allow much greater deployment of sensing with systems such as ours than are possible today.

5.9 System robustness

Although we showed our system works in the lab and for short-term field deployments, a long-term, real-world deployment raises a number of questions about system robustness. We next look at two questions related to system reliability under different conditions. Do environmental changes or sensor location affect our algorithm accuracy.

Table 3: Pipe temperature variation along time.

	T_u (℃)		T_d (℃)		ambient temp. (℃)	
time (s)	μ	σ	μ	σ	μ	σ
Noon	258	2.7	261	2.1	19	1.4
Evening	261	0.8	262	1.0	17	0.7
Midnight	258	1.0	263	1.0	10	0.23

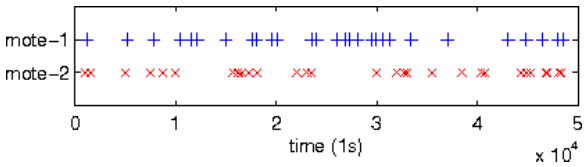

Figure 17: Mote radio packet loss distribution. Each marker represents one sample missing from data set.

5.9.1 Diurnal effects

In many locations, outside temperature can vary by 30 ℃ or more between day and night, and by 50 ℃ or more over the course of a year. We therefore looked at our system to evaluate if environmental temperature changes affect TEG or sensing performance.

During our overnight deployment the ambient temperature varied between a high of 22 ℃ and a recorded low of 9 ℃. However the system was up-and-running, without a single reboot, when we returned next morning. Hence our thermal harvester can demonstrably support the sensing application through-out the day, irrespective of the affects of the diurnal variation in ambient (and possibly pipe) temperature.

We then verify the correlation between pipe temperature we measured and ambient temperature, especially diurnal amplitude. We choose three time series sections to represent noon (12:30pm–1:00pm), evening (4:40pm–6:00pm) and midnight (11:00pm–0:40am) scenario, We discuss mean temperature first. The ambient temperature drops from 19 to 10 ℃ but pipe temperature remains relatively constant. Next we find that in day time the pipe temperature measured has more jitter than night time, according to the standard deviation comparison, but the difference is still insignificant. Up-stream co-generation power cycle or distribution branch valve is likely to have more impact. We finally conclude that there is no strong correlation between pipe temperature and diurnal amplitude and our pipe has similar temperature distribution at any time of the day. And hence, our algorithm should work all the time.

According to forgoing discussion, the diurnal amplitude does not interrupt TEG function and has no significant impact over pipe line temperature. We finally conclude that diurnal amplitude does not affect our system performs.

5.9.2 Radio transmission reliability

Next, we want to verify that the communication between our system and base station is reliably. Since we hide the mote antenna inside the pelican box to prevent potential environmental hazard to our device, we expect packet loss. The distance between base station and sensor is about 4 m.

Figure 5.9.2 clearly shows the distribution of transmission failure. Each red cross represents one packet loss and we infer the data from discontinuities in received packet sequence number. We find that the loss is uniform in the whole time space with slight burstiness. And no significant evidence shows that the loss of two motes is correlated. The total packet loss rate is 0.61% ($^{31}/_{4914}$) at mote-1 and 0.67% ($^{33}/_{4914}$) at mote-2. And we conclude that the wireless communication channel is robust enough to ensure base station meaningful data series.

5.9.3 Sensor location

Finally, exact sensor location can effect system operation. The physics of steam flow in a pipeline have unusual properties around points of constriction: a phenomenal known as *flashing*. Sensor placement can therefore affect results.

Figure 18 compares temperature fluctuation at different downstream spot (after valve) upon blockage. In order to clearly plotting all three series, we aggregated them by a 50-sample long window. T_d^1 is temperature right after valve. T_d^2 is after T_d^1 but before the choke and T_d^3 is after the choke. In gen-

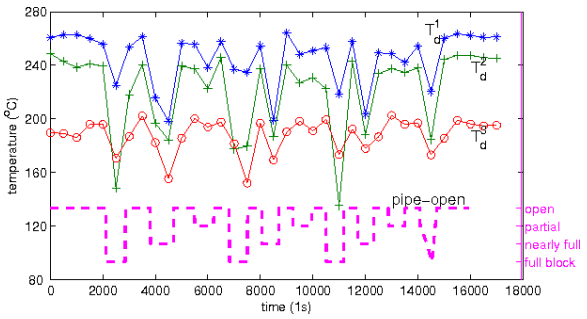

Figure 18: Aggregated all three down-stream temperature.

eral, all three series shows distinguishable drop at three level blockages, in different magnitude. However, more careful contrast reveals some other interesting results. Contrary to T_d^1 and T_d^3, T_d^2 shows that temperature upon full blockage is lower than that of nearly full blockage. The reason is that T_d^2 is farther down-stream than T_d^1 to the valve and hence the "choke flashing" transient after the valve or choke does not exist at T_d^2 but affects T_d^1 and T_d^3.

In all, we find that sensor placement affect result to some extent, but we may adjust our algorithm parameter to cope with peak ΔT value variation.

6 Related Work

Our work builds on prior research results in energy harvesting, ,change detection algorithms ,and sensor networks for industrial monitoring. We consider these areas in the following sections.

6.1 Energy Harvesting Systems

Energy harvesting for sensor network has been an active area of research. Today, electricity can be immediately harvested from several types of energy sources at a relatively low cost. These include light, wind, vibration, heat, magnetic, and radio [7]. Low-power sensor nodes can be powered by even a small fraction of ambient energy. Accordingly, there have been a number of research on scavenging ambient energy to operate wireless sensor nodes, some using traditional sources such as sunlight, vibration, and mechanical [35, 46, 32] while others using more exotic methods as body heat, radio fields, and multiple energy sources [28, 39, 37]

One of the first research in energy-harvester based sensornet used solar power to drive individual nodes [22, 44]. Heliomote was the first system to integrated solar-power and power conditioning to drive mote-class hardware [35]. We leverage this prior work and use a modified version of the heliomote to condition the output of our TEG. Prometheus replaced rechargeable batteries with supercapacitors to reduce energy loss during the conversion process [19]. AmbiMax platform further increased efficiency by performing maximum power point tracking (MPPT, essentially matching the source and load impedance) and adds multi-modal (solar and wind) energy harvesting [33]. Each of these prior platforms employ battery or supercapacitor to isolate energy harvesting from consumption. We show that this buffer can sometimes be eliminated or reduced.

Researchers have looked at optimizing the efficiency of energy harvested with large (25 W) waste water systems [38]) to lower power generators using automobile waste-heat(4 W) [29] and even for microgenerators that use soil-to-air thermal gradient generating a maximum of 0.35 W [26]. Our work provides a cost-efficient and energy-sufficient solution for powering an embedded system. Other researchers have investigated harvesting thermal energy for storage in energy buffers. Mateu *et al.* harvest about 5 mW using the thermal gradient between human body and ambient temperature but use NiMH battery to store energy [28]. Sodano et al. argues that TEG modules can generate greater power while charging batteries quicker than piezo-electric system under typical conditions [41]. Our work provides a batteryless solution and focuses on integrating thermal harvesting with sensing, optimized for low-power, low-cost, sensor network applications.

The Micropelt TE-node is most closely related to our work. The Micropelt platform low-power (sub-10 mW) sensor node [30] with an internal 100 μF capacitor for energy storage, with harvesting from a custom thermo-electrical generator [4, 3]. Our work

differs in that we use a general purpose senor platform, evaluating the potential and trade-offs for batteryless operation. We also explore a general purpose platform (running TinyOS) which allows us to experiment with variety of sensing and sensor fusion algorithms.

6.2 Change-point detection Algorithms

Many real-time monitoring systems use abrupt detection [2] or change-point detection [1] to detect problem from observed. For example, change point detection is used to detect anomalous behavior in Internet for the purpose of security [45]. Several change-point detection algorithm exist; many adapt exponential-weighted moving average (EWMA) because it is reliable, adaptive and easy to implement and configure [18, 43, 24].

Our mote software leverages the implementation of bit-shift-style EWMA. Trifa *et al.* develop an adaptive yellow bellied marmot alarm call detection algorithm based on EWMA of the environment noise monitoring [43]. Our work uses similar concepts to detect significant change in pipe skin temperature using EWMA. Kim *et al.* proposes several interesting EWMA-based algorithms to optimize streaming detection [24]. One of their algorithm, called flip flop filter, keeps both agile and stable EWMA and switches between the two to find the best baseline to use in the algorithm. Although our algorithm also maintains two EWMAs, we directly compare these two traces to detect sudden changes in temperature of the pipeline.

6.3 Pipeline monitoring systems

The key difference between a sensor in a traditional SCADA system and a sensor in a sensornet is that each sensornet node contains a programmable processor[31, 10]. The sensornet nodes are designed to be inexpensive and consume little power to operate. In a most traditional sense, wireless sensornet nodes are programmed to form a network and routes to efficiently sample and aggregate sensor data. Since these nodes are programmable, researchers have produced various useful applications over the last decade. Highly successful examples of the wireless sensor networks include UC Berkeley Motes and Smart Dust.

Most pipeline monitoring research works are targeting low-temperature, incompressible fluid [42, 25, 20, 40], while we are focusing on high temperature, high pressure and compressible steam. Besides, we employ a different sensing modality —temperature, while others do vibration or acoustic. Pipenet [42] prototypes an urban sewage monitoring system based on wireless sensor and demonstrates that they can detect water leakage by vibration frequency analysis. NAWMS [25] instead focusing on personal water usage. Although they use similar hardware, but their linear programming based algorithm is still different from ours. Jin *et al.* [20] and Sinha [40] both exploit acoustic sensor for pipe line monitoring. Jin focuses on a general sensor network platform while Sinha's work is mainly about instrumentation and calibration.

Zhu's work relates to ours most in terms of sensing modality and target fluid. He shows the feasibility of temperature monitoring for blockage detection of pulverized coal injection system [48]. He mount thermometers on branch pipes to furnace and run detection algorithm based on temperature variation along pipe. His algorithm takes input of instantaneous pipe skin temperature and up/downstream ΔT, ignoring long-term trend, and then compares them to preconfigured thresholds. Our approach is similar, but we examine ΔT alone to avoid extra configuration and employ long-term EWMA to build baseline in order to be adaptive. Finally, we use inexpensive and portable hardware (less than US$600) comparing to his centralized system. Although not explicitly mentioned in his paper, we estimate it is likely to cost around US$1000 for industry control computer, specialized signal processing module and signal transmission wires. Additionally, our system has potentially good scalability and low deployment cost.

We described the potential of sensor networks in oilfield production systems previously [47]. While that work identifies the potential, in this paper we demonstrate a field-tested system, evaluate specific sensing algorithms, and demonstrate that the whole

system can operate on steam-power.

7 Conclusions

We have described a system for steam-powered sensing to detect pipeline blockages. The work showed the potential to power a sensor network by the phenomena being sensed, to operate without any battery. We developed an algorithm to detect problems in pipelines using non-invasive sensing. We have demonstrated the effectiveness of this system and its components through laboratory tests and field experiments. Although we have developed this system to match the needs of sensing blockage in steam distribution networks, the principles of thermal energy harvesting and non-invasive sensing apply to a range of industrial sensing applications.

Acknowledgments

We would like to thank Jonathan Friedman for his help using ATLA Labs' Heliomote.

We thank Greg LaFramboise, Charlie Webb, Mohammad Heidari for their input on Chevron's business requirements and field conditions; David Menda for input into the project, and Iraj Erhagi, Mike Hauser as co-directors of CiSoft.

References

[1] V. Veeravalli A. Tartakovsky. Change-point detection in multichannel and distributed systems with applications. In *Applications of Sequential Methodologies*, pages 331–363. Marcel Dekker, Inc., 2004.

[2] Michèle Basseville and Igor V. Nikiforov. *Detection of abrupt changes: theory and application*. Prentice-Hall, Inc., Upper Saddle River, NJ, USA, 1993.

[3] H. Bottner. Micropelt miniaturized thermoelectric devices. In *Proceedings of ICT, Clemson, SC*, 2005.

[4] H. Bottner, J. Nurnus, M. Braun, J. Wollenstein, F. Volkert, and A. Schubert. MicroPelt: state of the art, road map and applications. Technical report, Infineon Technologies AG, Munchen, Germany, 2004.

[5] Roger M. Butler. *Thermal Recovery of Oil and Bitumen*. Prentice-Hall, 1997.

[6] M. Calle and J. Kabara. Measuring energy consumption in wireless sensor networks using gsp. In *Personal, Indoor and Mobile Radio Communications, 2006 IEEE 17th International Symposium on*, pages 1–5, Sept. 2006.

[7] A. Chandrakasan, R. Amirtharajah, Seonghwan Cho, J. Goodman, G. Konduri, J. Kulik, W. Rabiner, and A. Wang. Design considerations for distributed microsensor systems. In *Custom Integrated Circuits, 1999. Proceedings of the IEEE 1999*, pages 279–286, 1999.

[8] Crane Co. *Flow of Fluids through Valves, Fittings, and Pipe*. Technical Paper No 410, Crane Company, 1988.

[9] Harold L. Cook and H. F. Dotterweich. *Report on calibration of positive flow beans manufactured by Thornhill-Craver Company, inc.* Texas College of Arts and Industries, 1946.

[10] A. Daneels and W. Salter. What is SCADA? In *Proceedings on the International Conference on Accelerator and Large Experimental Physics Control System*, 1999.

[11] Western Electric. *Statistical Quality Control Handbook*. Western Electric Corporation, Indianapolis, Inc., 1956.

[12] American Society for Testing and Materials. *A Manual on the Use of Thermocouples in Temperature Measurement, fourth edition*. ASTM, Philadelphia, 1993.

[13] Suzanne Griston and Tom Abate. Field test of taperedbore for steam flow control. In *SPE Western Regional Meeting*, pages 269–283, Anchorage, AK, USA, May 1996. Society of Petroleum Engineers. (SPE 35677).

[14] H. Hayashi, Y. Takabayashi, H. Tsuji, and M. Oka. Rapidly increasing application of intranet technologies for SCADA (supervisory control and data acquisition system). In *IEEE/PES Transmission and Distribution Conference and Exhibition 2002: Asia Pacific*, volume 1, 2002.

[15] http://www.customthermoelectric.com/. Custom Thermoelectric.

[16] http://www.vernier.com/go/gotemp.html. Vernier go!temp thermometer.

[17] Hans H. A. Huygen and J. L. Huitt. Wellbore heat losses and casing temperatures during steam injection. *Drilling and Production Practice*, 1966.

[18] V. Jacobson. Congestion avoidance and control. In *SIGCOMM '88: Symposium proceedings on Communications architectures and protocols*, pages 314–329, New York, NY, USA, 1988. ACM.

[19] Xiaofan Jiang, Joseph Polastre, and David Culler. Perpetual environmentally powered sensor networks. In *IPSN '05: Proceedings of the 4th international symposium on Information processing in sensor networks*, page 65, Piscataway, NJ, USA, 2005. IEEE Press.

[20] Yuanwei Jin and Ali Eydgahi. Monitoring of distributed pipeline systems by wireless sensor networks. In *Proceedings of The 2008 IAJC-IJME International Conference*, 2008.

[21] Velimir Jovanovic and Saeid Ghamaty. Design, fabrication, and testing of energy-harvesting thermoelectric generator. *Smart Structures and Materials 2006: Smart Structures and Integrated Systems*, 6173(1):61730G, 2006.

[22] A. Kansal and M. B. Srivastava. An environmental energy harvesting framework for sensor networks. In *The 2003 international symposium on Low power electronics and design*, pages 481–486, Seoul, Korea, 2003. ACM Press.

[23] Aman Kansal, Jason Hsu, Sadaf Zahedi, and Mani B. Srivastava. Power management in energy harvesting sensor networks. *ACM Trans. Embed. Comput. Syst.*, 6(4):32, 2007.

[24] Minkyong Kim and Brian Noble. Mobile network estimation. In *MobiCom '01: Proceedings of the 7th annual international conference on Mobile computing and networking*, pages 298–309, New York, NY, USA, 2001. ACM.

[25] Younghun Kim, Thomas Schmid, Zainul M. Charbiwala, Jonathan Friedman, and Mani B. Srivastava. Nawms: nonintrusive autonomous water monitoring system. In *SenSys '08: Proceedings of the 6th ACM conference on Embedded network sensor systems*, pages 309–322, New York, NY, USA, 2008. ACM.

[26] E.E. Lawrence and G.J. Snyder. A study of heat sink performance in air and soil for use in a thermoelectric energy harvesting device. In *Thermoelectrics, 2002. Proceedings ICT '02. Twenty-First International Conference on*, pages 446–449, Aug. 2002.

[27] Loreto Mateu, Cosim Codrea, Nestor Lucas, Markus Pollak, and Peter Spies. Human body energy harvesting thermogenerator for sensing applications. In *SENSORCOMM '07: Proceedings of the 2007 International Conference on Sensor Technologies and Applications*, pages 366–372, Washington, DC, USA, 2007. IEEE Computer Society.

[28] Loreto Mateu, Cosim Codrea, Nestor Lucas, Markus Pollak, and Peter Spies. Human body energy harvesting thermogenerator for sensing applications. *Sensor Technologies and Applications, International Conference on*, 0:366–372, 2007.

[29] K. Matsubara. Development of a high efficient thermoelectric stack for a waste exhaust heat recovery of vehicles. In *Thermoelectrics, 2002. Proceedings ICT '02. Twenty-First International Conference on*, pages 418–423, 2002.

[30] Micropelt. TE-power node: Self-sufficient wireless sensor system thermoharvesting explorer. Product datasheet, March 2010.

[31] F. J Molina, J. Barbancho, and J. Luque. Automated meter reading and SCADA application for wireless sensor network. *Ad-Hoc, Mobile, and Wireless Networks*, pages 223–234, 2003.

[32] J. A. Paradiso and T. Starner. Energy scavenging for mobile and wireless electronics. *Pervasive Computing, IEEE*, 4(1):18–27, 2005.

[33] Chulsung Park and P.H. Chou. Ambimax: Autonomous energy harvesting platform for multi-supply wireless sensor nodes. In *Sensor and Ad Hoc Communications and Networks, 2006. SECON '06. 2006 3rd Annual IEEE Communications Society on*, volume 1, pages 168–177, Sept. 2006.

[34] R.H. Perry and D.W. Green. *Perry's Chemical Engineers' Handbook, Sixth Edition*. McGraw-Hill, 1984.

[35] V. Raghunathan, A. Kansal, J. Hu, J. Friedman, and M. Srivastava. Design considerations for solar energy harvesting wireless embedded systems. In *4th international symposium on Information processing in sensor networks*, 2005.

[36] Gerald Recktenwald. Conversion of thermocouple voltage, 2006.

[37] Shad Roundy, Brian P. Otis, Yuen hui Chee, Jan M. Rabaey, and Paul Wright. A 1.9ghz rf transmit beacon using environmentally scavenged energy. In *Dig. IEEE Int. Symposium on Low Power Elec. and Devices, Seoul, Korea*, 2003.

[38] M.D. Rowe, Gao Min, S.G.K. Williams, A. Aoune, K. Matsuura, V.L. Kuznetsov, and Li Wen Fu. Thermoelectric recovery of waste heat-case studies. In *Energy Conversion Engineering Conference, 1997. IECEC-97., Proceedings of the 32nd Intersociety*, pages 1075–1079 vol.2, Jul-1 Aug 1997.

[39] Alanson Sample and Joshua R. Smith. Experimental results with two wireless power transfer systems. Technical report, Intel Research and University of Washington, 2009.

[40] Dipen Sinha. Acoustic sensor for pipeline monitoring. Technical report, Los Alamos National Laboratory, July 2005.

[41] Henry A. Sodano, Garnett E. Simmers, Remi Dereux, and Daniel J. Inman. Recharging batteries using energy harvested from thermal gradients. *Journal of Intelligent Material Systems and Structures*, 18(1):3–10, 2007.

[42] Ivan Stoianov, Lama Nachman, Sam Madden, and Timur Tokmouline. Pipeneta wireless sensor network for pipeline monitoring. In *IPSN '07: Proceedings of the 6th international conference on Information processing in sensor networks*, pages 264–273, New York, NY, USA, 2007. ACM.

[43] Vladimir Trifa, Lewis Girod, Travis Collier, Daniel T Blumstein, and Charles E. Taylor. Automated wildlife monitoring using self-configuring sensor networks deployed in natural habitats. In *International Symposium on Artificial Life and Robotics (AROB07)*, Beppu, Japan, January 2007.

[44] Thiemo Voigt, Hartmut Ritter, and Jochen Schiller. Utilizing solar power in wireless sensor networks. In *LCN '03: Proceedings of the 28th Annual IEEE International Conference on Local Computer Networks*, page 416, Washington, DC, USA, 2003. IEEE Computer Society.

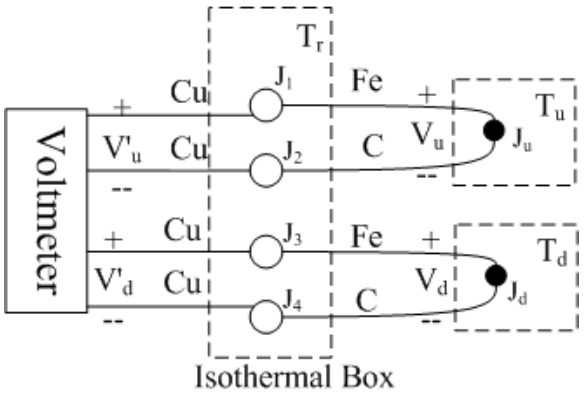

Figure 19: Two J type thermocouples with reference junctions.

[45] Haining Wang, Danlu Zhang, and Kang G. Shin. Change-point monitoring for the detection of dos attacks. *IEEE Trans. Dependable Secur. Comput.*, 1(4):193–208, 2004.

[46] C. B. Williams and R. B. Yates. Analysis of a micro-electric generator for microsystems. In *Solid-State Sensors and Actuators, 1995 and Eurosensors IX.. Transducers '95. The 8th International Conference on*, volume 1, pages 369–372, 1995.

[47] SunHee Yoon, Wei Ye, John Heidemann, Brian Littlefield, and Cyrus Shahabi. SWATS: Wireless sensor networks for steamflood and waterflood pipeline monitoring. *IEEE Network Magazine*, 2009. accepted in 2009 to appear in 2010 or later.

[48] Jin-ming Zhu. Application of temperature method for jam detection in BF coal injection. *Baosteel Technology 2005-6*, 2005.

A Proof of reference point temperature cancellation

In Section 5.3 we assert that we do not have to calibrate the reference point temperature on thermocouple We here provide a formal proof about how the errors from two thermocouples cancel each other, assuming both in the same isothermal box.

Figure 19 shows a J-type thermocouple connection. Here V_u and V_d are the voltage generated by T_u and T_d at J_u and J_d.[2] while there are other four reference junctions to voltmeter in a isothermal box. V'_u and V'_d are the actual voltmeter readings. If we compare theoretically real thermocouple voltage output ΔV against practical voltmeter readings $\Delta V'$, we have

$$\begin{aligned}
\Delta V &= V_u - V_d \\
&= \rho(T_u) - \rho(T_d) \\
V'_u &= \rho(T_u - T_r) \\
V'_d &= \rho(T_d - T_r) \\
\Delta V' &= V'_u - V'_d \\
&= \rho(T_u - T_r) - \rho(T_d - T_r) \\
&= \rho(T_u - T_d) + \rho(T_r - T_r) \\
&= \rho(T_u) - \rho(T_d) \\
&= \Delta V
\end{aligned}$$

And ρ is the thermocouple pseudo-coefficient. The reference junction errors from two thermocouple cancel each other if we ensure that they are all in a isothermal box. More clearly, when two reference junction pair (J_1 and J_2 against J_3 and J_4) has the same metal combination under same temperature, their voltage potential is constantly equal.

B Parameter sensitivity of the basic sensing algorithm

Section 5.4 and Section 5.5 have shown that our algorithm is able to detection steam choke blockage under certain parameter settings. We next study how sensitive those results are to the parameters settings, to learn how tolerant the application is to different situations or potential misconfiguration

Figure 20 shows our algorithm performance with different upper threshold (*th_block*). Short- and long-term EWMA gain is fixed to $1/2$ and $1/16$ respectively for this analysis according to Section 4.4. We configure $\alpha_l < 1/64$ to reset the long-term history to

[2] For modeling simplicity, we treat the voltage potential along different wires as a single point voltage source, although this is a common misunderstanding that voltage is generated entirely at the soldering junction of dissimilar material. In reality, voltage or electromotive force is introduced by the temperature gradient along each wire separately. Differences ins wire material leads to the voltage difference between the two ends when the wires are connected.

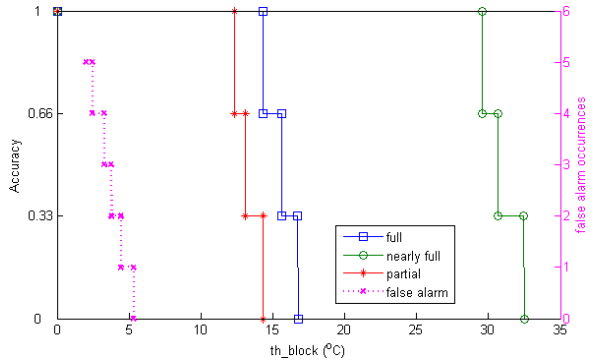

Figure 20: Accuracy and false alarm at different *th_block* ($\alpha_l = 1/16$) .

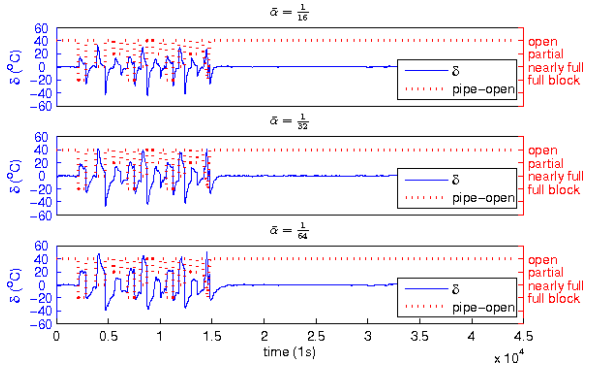

Figure 21: δ fluctuation influenced by different α_l.

normal level between any two controlled blockages We have examined choices both long- and short-term gain (evaluation omitted due to space) and believe that these parameters are suitable for our application. The whole experiment give us three times for each type of blockage and we are also presenting false alarms when *th_block* ≥ 2 ℃.

We draw two observations from Figure 5. First, carelessly configured parameter triggers false alarms. An over-aggressive *th_block* value (≤ 5.3 ℃) would mistake normal temperature fluctuation for pipe anomaly. However, one could easily avoid the problem by taking temperature intrinsic property in account, e.g. mean and deviation. Finally, our algorithm is not sensitive to long-term ΔT history gain, α_l, as long as it is reasonably small. Figure 21 shows that larger α_l yields higher δ peak, because long-term history are more sluggish, but also takes more time to subside when pipe back to normal. However, according to those δ peak values, it is easy to optimize parameter set for all 3 α_l's.

In all, we conclude that our algorithm is sensitive to detection threshold but not to history gains. However, parameter configuration is still easy and We find a range of parameters to yield 100% accuracy and limited detection delay within limits.

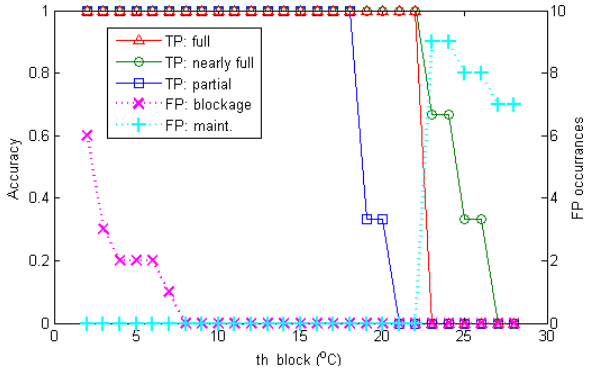

Figure 22: Evaluation of improved algorithm running between T_u and T_d^1 for choke blockage detection. *th_maint* is fixed at 16 ℃.

C Parameter sensitivity of the extended algorithm

Section 5.5 shows that our extended algorithm successfully avoids false alarms caused by pipe maintenance. Similar to the sensitivity evaluation of the basic algorithm (Section B), we next study the extended algorithm's robustness to parameter variations. We apply our algorithm to two different sensor pairs and evaluate blockage and maintenance threshold separately.

We first evaluate our improved algorithm parameter sensitivity between T_u and T_d^1, straddling the valve for blockage detection scenario. Our hypothe-

sis is that the new algorithm should performs similar to the base algorithm, or better. We fix *th_maint* at 16 ℃ to simplify the analysis, since this parameter is not critical for blockage detection (Likewise, we set *th_block* as 16 ℃ in the next scenario evaluation). This number is not randomly chosen, we prove that it works well for MAINTENANCE detection and is good for our algorithm robustness test. Figure 22 shows that generally, the algorithm tweak does not affect the detection of this scenario comparing to Figure 20, although we have some MAINTENANCE false alarms. We still find a range of *th_block*, [8, 18], which yields perfect detection — 100% detection accuracy for all three level of blockage and 0 false alarm occurrence. Another similarity is that larger threshold makes it harder to trigger detections and the system fails all detections if $th\_block \geq 27$.

We separate two kinds of false alarms — false blockage and false MAINTENANCE into two dotted lines in Figure 22 and discuss them here. Similar to the base algorithm, an over-aggressive (small) threshold is likely to mistake signal series jitters for blockage anomaly. But a reasonable parameter configuration, $th\_block \geq 8$ easily eliminates the problem. The occurrence of MAINTENANCE false positive is because of the asynchronous history variation. Upon blockage, both short- and long-term history would rise in different speed but parameter misconfiguration ($th\_block \geq 22$) may prevent the system detects at the first time. After a certain time, if the anomaly settles, the drop of ΔT would make short-term history drops below long-term history. This δ valley would then be captured by the system and report as MAINTENANCE.

We next evaluate the algorithm on T_d^2 and T_d^3, straddling the actual choke. Our hypothesis is that since the valve is far upstream to the both spots and we use it for blockage simulation, our algorithm should be able to distinguish this anomaly from choke blockage. Figure 23 shows that the algorithm successfully detects the MAINTENANCE scenario at reasonable false alarm rate. The first observation is a smaller perfect detection parameter range — [15,17] of *th_maint*, comparing to the previous case. However, we believe this problem is fundamentally harder than choke blockage scenario for two reasons. First,

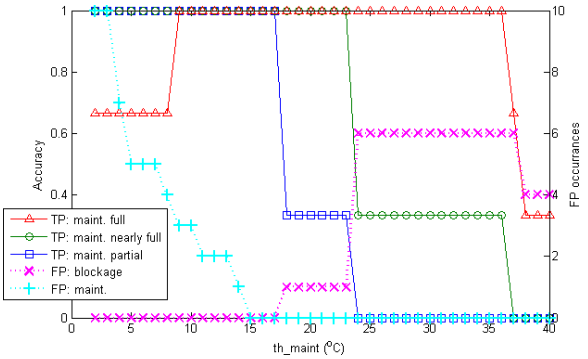

Figure 23: Evaluation of improved algorithm running between T_d^2 and T_d^3 for MAINTENANCE detection. *th_block* is fixed at 15 ℃.

for MAINTENANCE the inertia of the choke cause more unpredictable ΔT variations, which is the purpose of the choke — regulating and separate downstream pressure from the upper one. The other is that valve is relatively farther to the two sensors and we believe distance somehow absorbs the valve operation impact and incur more noise to the data (briefly discussed in Section 5.9.3). Therefore, parameter misconfiguration, say $th\_maint \leq 7$ or $th\_maint \geq 24$ triggers a certain number of false blockage or MAINTENANCE alarms. Another observation is that, contrary to previous scenario, full upstream blockage is the easiest to detect, easier than nearly-full. The reason is similar to that of the last observation, two sensor are far downstream to the blockage spot and the choke effect subsides. The full blockage creates the most ΔT drop while partial one has only insignificant.

We carefully evaluate our improved algorithm in two different scenario — blockage and upstream maintenance with temperature data straddling the valve and the choke. We demonstrate that our algorithm yields good accuracy and reasonable false alarms in a wide range of parameters for steam pipe.